Supporting Information

Dual active nitrogen doped hierarchical porous hollow carbon nanospheres as oxygen reduction electrocatalyst for zinc-air batteries

Jiawei Zhu[a], Huang Zhou[a], Chengtian Zhang[a], Jian Zhang[a,b]* and Shichun Mu[a]*

[a]State Key Laboratory of Advanced Technology for Materials Synthesis and Processing, Wuhan University of Technology, Wuhan 430070, China

[b]State Key Laboratory of Material Processing and Die & Mould Technology, School of Materials Science and Engineering, Huazhong University of Science and Technology, Wuhan 430074, PR China

Fax: +86 27 87879468.

E-mail: msc@whut.edu.cn, zhangjian7@hust.edu.cn.

Equation S1

The rotating ring-disk electrode (RRDE) measurements for the catalyst were also performed with a three-electrode system in O_2-saturated 0.1 M KOH solution at a rotation rate of 1600 rpm with a scan rate of 10 mV s^{-1}, and the potential of the Pt ring was set at V = 1.5 V. The apparent electrons transferred numbers were calculated based on the following equation:

$$n=4J_D / (J_D + J_R / N) \quad (1)$$

where J_D and J_R represent the disk and ring currents, respectively. And N is the current collection efficiency of the Pt ring, which was 0.37 in our system.

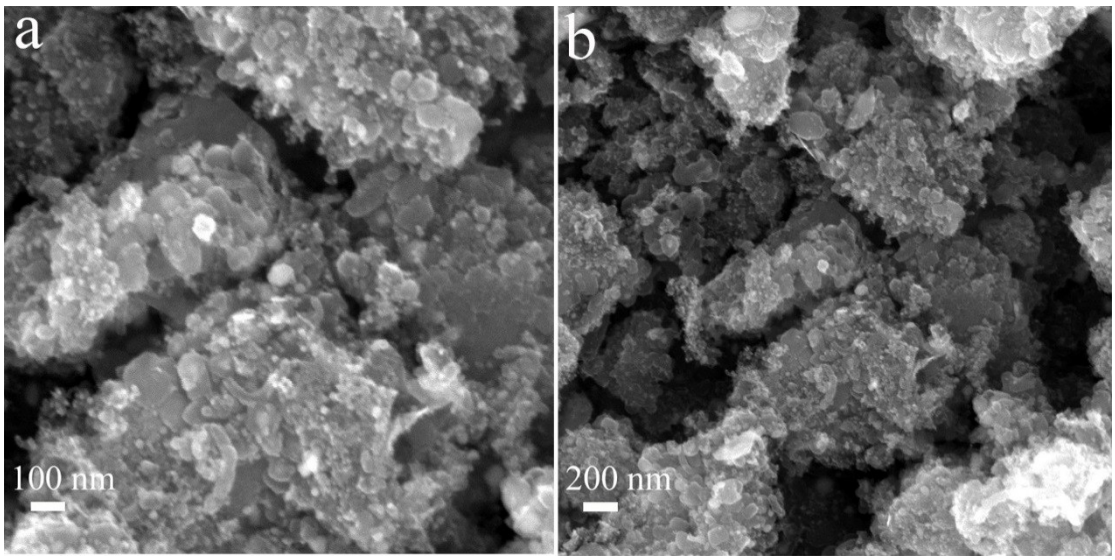

Figure S1 (a, b) SEM images for N-BC.

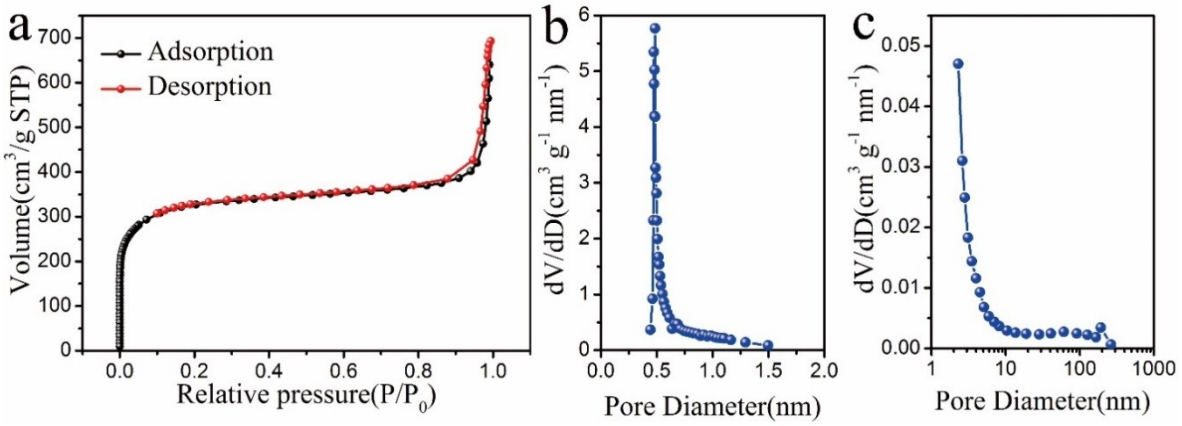

Figure S2 (a) N_2 adsorption-desorption isotherm and (b, c) pore size distribution plots for N-BC.

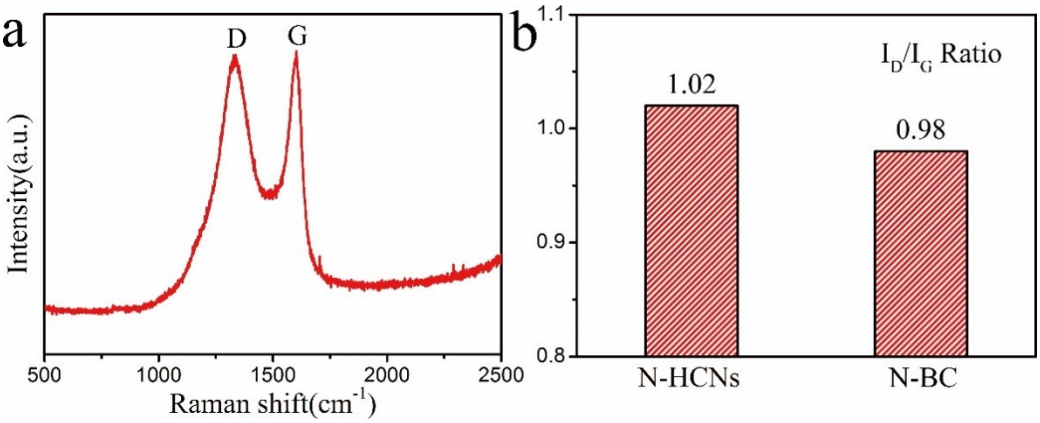

Figure S3 (a) Raman spectrum for N-BC; (b) peak intensity ratios of the D band to the G band (I_D/I_G) for N-HCNs and N-BC.

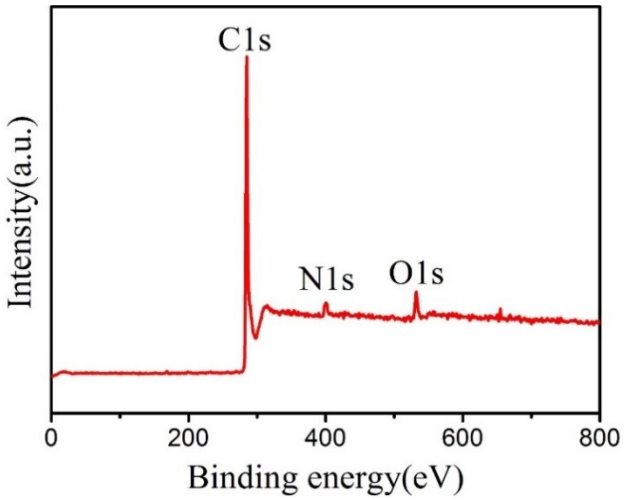

Figure S4 XPS survey spectrum of the N-HCNs.

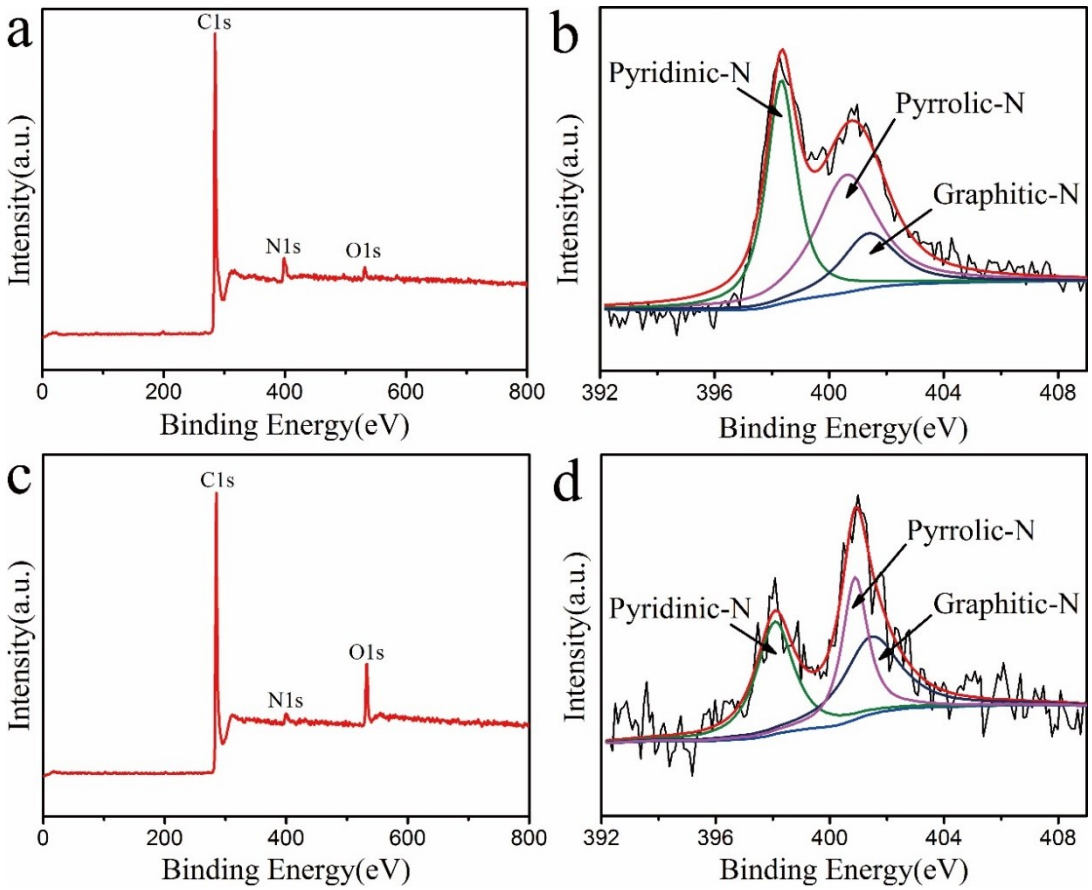

Figure S5 XPS survey spectra of the (a) N-BC and (c) N-MPC; curve-fitted N1s spectra for (b) N-BC and (d) N-MPC.

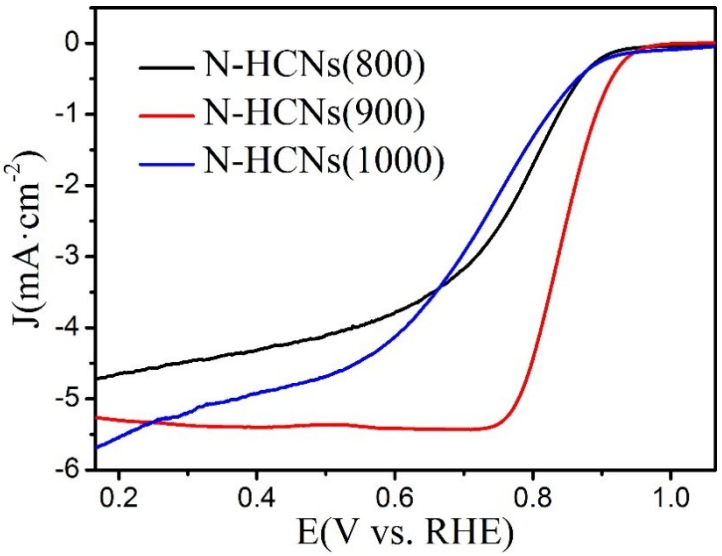

Figure S6 LSV curves for samples pyrolyzed at different temperatures.

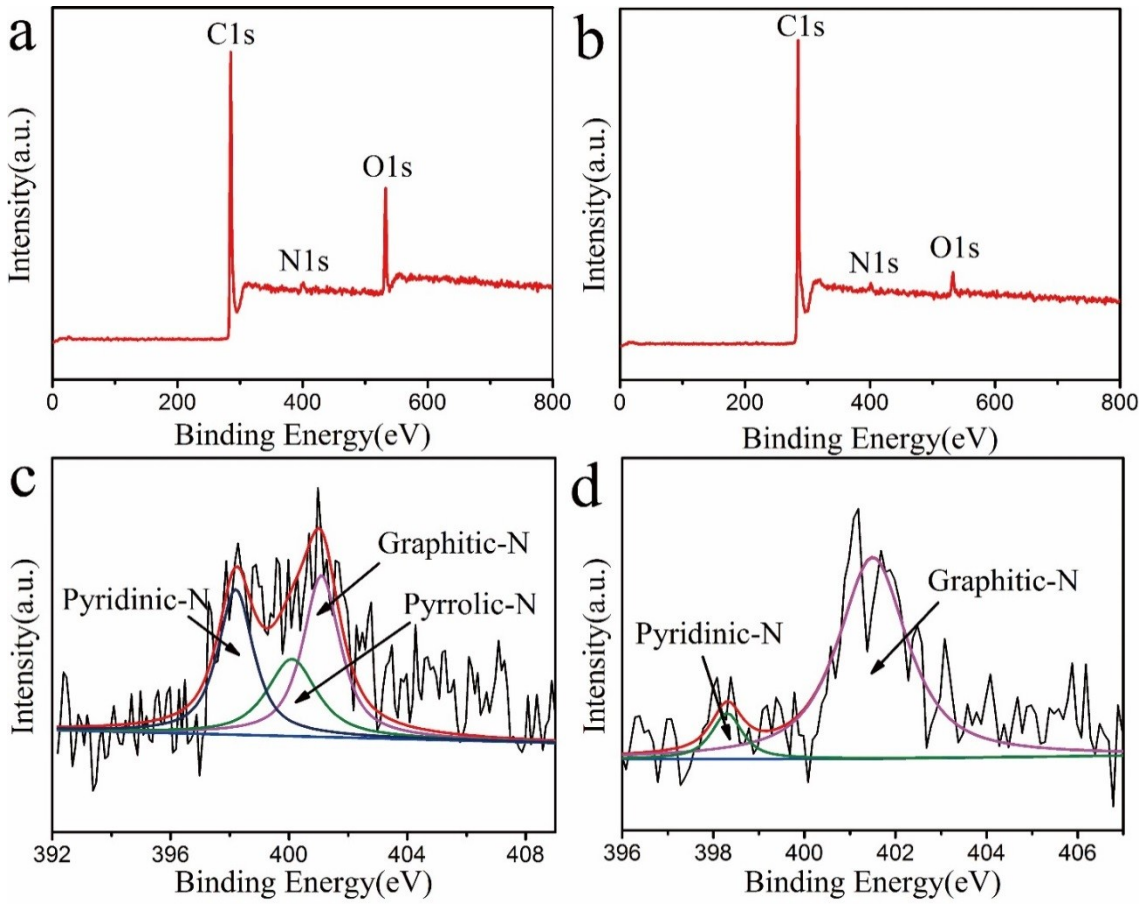

Figure S7 XPS survey spectra for (a) N-HCNs (800) and (b) N-HCNs (1000); curve-fitted N1s spectra for (c) N-HCNs (800) and (d) N-HCNs (1000).

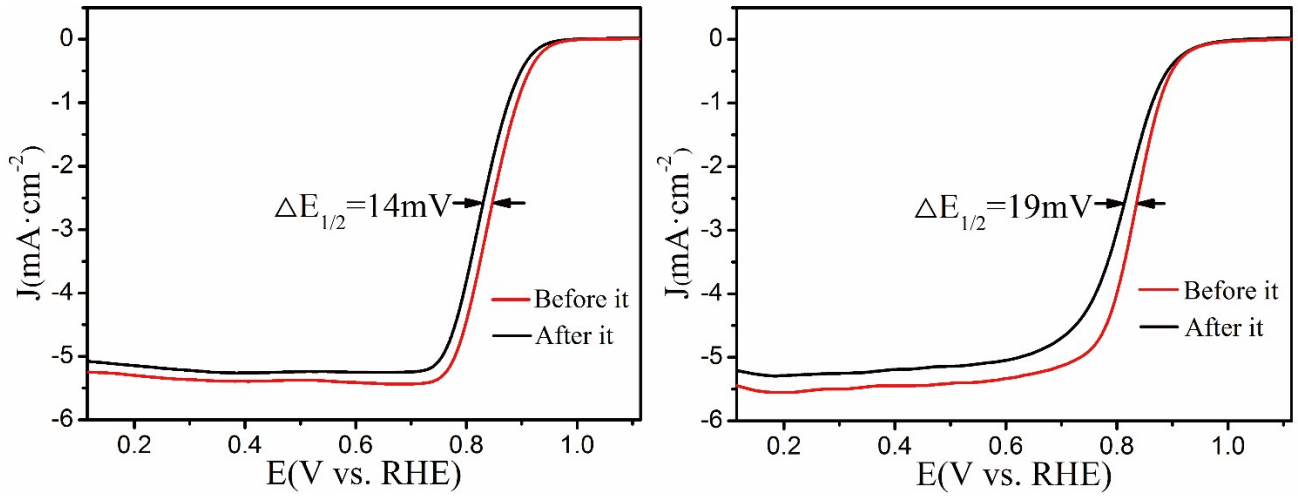

Figure S8 LSV curves at 1600 rpm before and after i-t chronoamperometric responses for (a) N-HCNs and (b) Pt/C.

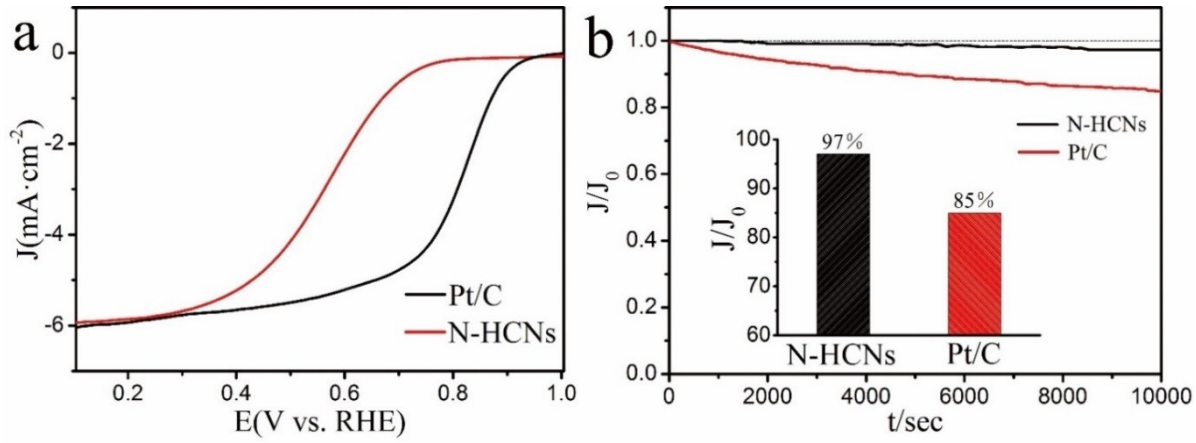

Figure S9 (a) LSV curves for N-HCNs and Pt/C catalysts at 1600 rpm in 0.1 M $HClO_4$ solutions; (b) the i-t chronoamperometric responses for N-HCNs and Pt/C in acidic media.

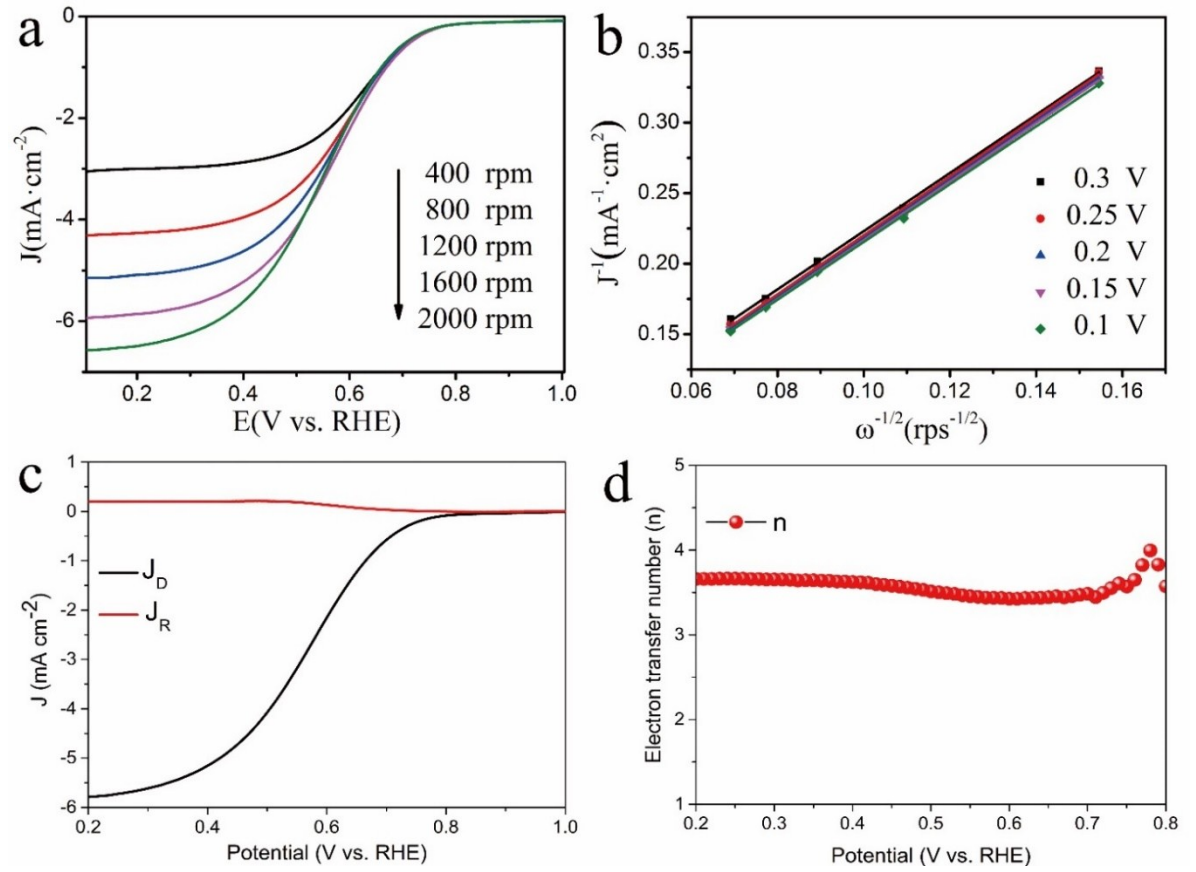

Figure S10 (a) LSV curves and (b) Koutecky-Levich (K-L) plots for N-HCNs at various rotating rates from 400 to 2000 rpm in acidic media (n≈ 4.23); (c) RRDE polarization curves

at 1600 rpm for the N-HCNs catalyst in 0.1 M $HClO_4$; (d) the calculation results of the electron transfer number.

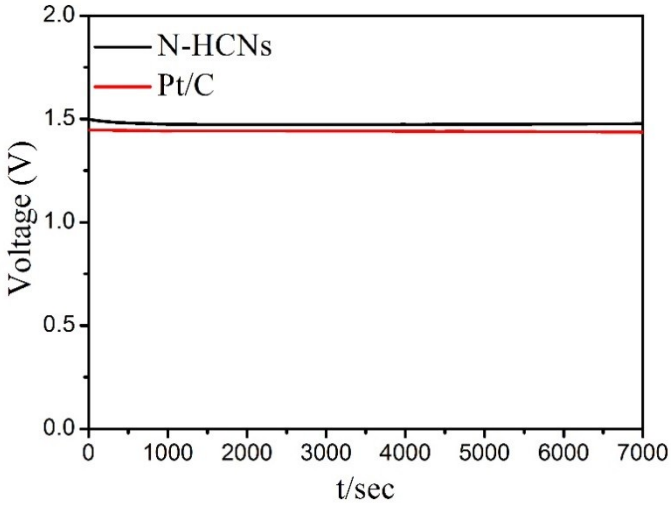

Figure S11 Open circuit voltage vs. time curves of the zinc–air battery with N-HCNs and Pt/C air electrode.

Table S1 Energy dispersive spectrometer analysis of N-HCNs.

Point	C/at.%	N/at.%	O/at.%
1	90.33	3.60	6.07
2	92.72	4.12	3.16
3	87.32	5.09	7.60
average	90.12	4.27	5.61

Table S2 Comparisons of ORR performance for N-HCNs with other reported N-doped carbon and M-Nx/C catalysts in 0.1 M KOH electrolytes.

Catalyst	**E_0/V**	**$E_{1/2}$/V**	**Ref.**
N-HCNs	0.931	0.845	This work
NDPG	0.9346	0.8346	1
EDA-NCNT	-	0.8153	2
N-HCNPs	0.8853	-	3
S-Fe/N/C	0.911	0.799	4
Fe-N/C-800	0.923	0.809	5
PANI-4.5Fe-HT2(SBA-15)	0.95	0.84	6
FePhenMOF-$ArNH_3$	0.98	0.78	7
Fe3-NG	0.965	0.826	8
Fe_3C@NG800-0.2	0.98	0.81	9
Fe-N70%/C-800	0.91	-	10
Fe-N-GC-900	1.01	0.86	11
HNCS71	0.97	0.82	12
FeNC-20-1000	1.04	0.88	13
Fe/Fe_3C@N-C-NaCl	0.970	0.869	14
Fe/N/G-0.25	0.98	0.84	15
Fe-N-CC	0.94	0.83	16
Fe-N/MCNs	0.95	0.83	17
Carbon-nanoshell	0.98	0.85	18
Fe-N/MC@0.6	1.01	0.88	19
Fe-N-C	0.83	0.72	20

References

1. H. Zhou, J. Zhang, J. Zhu, Z. Liu, C. Zhang and S. Mu, *Rsc. Adv*, 2016, **6**, 73292-73300.
2. Z. Chen, D. Higgins, H. Tao, R. S. Hsu and Z. Chen, *J. Phys. Chem. C*, 2014, **113**, 21008-21013.
3. G. Ma, R. Jia, J. Zhao, Z. Wang, C. Song, S. Jia and Z. Zhu, *J. Phys. Chem. C*, 2015, **115**, 25148–25154.
4. K. Hu, L. Tao, D. Liu, J. Huo and S. Wang, *ACS Appl. Mater. Inter.*, 2016, **8**, 19379–19385.
5. L. Lin, Q. Zhu and A. W. Xu, *J. Am. Chem. Soc.*, 2014, **136**, 11027-11033.
6. X. H. Yan and B. Q. Xu, *J. Mater. Chem. A*, 2014, **2**, 8617-8622.
7. J. Li, G. Shraboni, W. Liang, M. T. Sougrati, F. Jaouen, H. Barr, M. K. Samuel, M. C. Geoff, C. Ma and X. Yuan, *Energ Environ. Sci.*, 2016, **9**, 2418-2432.
8. X. Cui, S. Yang, X. Yan, J. Leng, S. Shuang, P. M. Ajayan and Z. Zhang, *Adv. Funct. Mater.*, 2016, **26**, 5708-5717.
9. H. Jiang, Y. Yao, Y. Zhu, Y. Liu, Y. Su, X. Yang and C. Li, *ACS Appl. Mater. Inter.*, 2015, **7**, 21511-21520.
10. Q. Cui, S. Chao, P. Wang, Z. Bai, H. Yan, K. Wang and L. Yang, *Rsc. Adv*, 2014, **4**, 12168-12174.
11. A. Kong, X. Zhu, Z. Han, Y. Yu, Y. Zhang, B. Dong and Y. Shan, *ACS Catal.*, 2014, **4**, 1793-1800.
12. J. Sanetuntikul, C. Chuaicham, Y.-W. Choi and S. Shanmugam, *J. Mater. Chem. A*, 2015, **3**, 15473-15481.
13. T. Liu, P. Zhao, X. Hua, W. Luo, S. Chen and G. Cheng, *J. Mater. Chem. A*, 2016, **4**, 11357-11364.
14. Y. Zhang, L. B. Huang, W. J. Jiang, X. Zhang, Y. Y. Chen, Z. Wei, L. J. Wan and J. S. Hu, *J. Mater. Chem. A*, 2016, **4**, 7781-7787.
15. C. Domínguez, F. J. Pérezalonso, M. A. Salam, S. A. Althabaiti, M. A. Peña, L. Barrio and S. Rojas, *J. Mater. Chem. A*, 2015, **3**, 24487-24494.
16. G. A. Ferrero, K. Preuss, A. Marinovic, A. B. Jorge, N. Mansor, D. J. Brett, A. B. Fuertes, M. Sevilla and M. M. Titirici, *ACS Nano*, 2016, **10**, 5922-5932.
17. J. Wei, Y. Liang, X. Zhang, G. P. Simon, D. Zhao, J. Zhang, S. Jiang and H. Wang, *Nanoscale*, 2015, **7**, 6247-6254.
18. Y. Wang, A. Kong, X. Chen, Q. Lin and P. Feng, *ACS Catal.*, 2015, **5**, 3887–3893.
19. S. Wang, M. Zhu, X. Bao, J. Wang, C. Chen, H. Li and Y. Wang, *Chemcatchem*, 2015, **7**, 2937–2944.

20. L. Osmieri, R. Escudero-Cid, A. H. A. M. Videla, P. Ocón and S. Specchia, *Appl. Catal. B-Environ.*, 2017, **201**, 253-265.